

# VDB-GPDF: Online Gaussian Process Distance Field with VDB Structure

Lan Wu<sup>1</sup>, Cedric Le Gentil<sup>1</sup>, and Teresa Vidal-Calleja<sup>1</sup>

**Abstract**—Robots reason about the environment through dedicated representations. Popular choices for dense representations exploit Truncated Signed Distance Functions (TSDF) and Octree data structures. However, TSDF is a projective signed distance obtained directly from depth measurements that overestimates the Euclidean distance. Octrees, despite being memory efficient, require tree traversal and can lead to increased runtime in large scenarios. Other representations based on Gaussian Process (GP) distance fields are appealing due to their probabilistic and continuous nature, but the computational complexity is a concern. In this paper, we present an online efficient mapping framework that seamlessly couples GP distance fields and the fast-access VDB data structure. This framework incrementally builds the Euclidean distance field and fuses other surface properties, like intensity or colour, into a global scene representation that can cater for large-scale scenarios. The key aspect is a latent Local GP Signed Distance Field (L-GPDF) contained in a local VDB structure that allows fast queries of the Euclidean distance, surface properties and their uncertainties for arbitrary points in the field of view. Probabilistic fusion is then performed by merging the inferred values of these points into a global VDB structure that is efficiently maintained over time. After fusion, the surface mesh is recovered, and a global GP Signed Distance Field (G-GPDF) is generated and made available for downstream applications to query accurate distance and gradients. A comparison with the state-of-the-art frameworks shows superior efficiency and accuracy of the inferred distance field and comparable reconstruction performance. The accompanying code will be publicly available<sup>3</sup>.

**Keywords:** Gaussian Process Distance Field, OpenVDB, Euclidean Distance Field, Gradient Field, Mapping.

## I. INTRODUCTION

Robots understand and interact with the world in a meaningful and efficient manner via effective representations. Building a representation that underpins perception, control, navigation, learning, and manipulation is fundamental but has key requirements that include: 1) high accuracy to reflect the true nature of the unknown environment, 2) efficiency to allow online performance, 3) scalability to handle large-scale scenarios, 4) adaptability to deal with dynamic changes, 5) compatibility with varying sensors, 6) flexibility to provide the needed output space, 7) robustness to ensure reliable operation in the presence of noise and 8) being dense and potentially generative to deal with incomplete and discrete data.

<sup>1</sup>All authors are with the Robotics Institute, Faculty of Engineering and IT, University of Technology Sydney, Ultimo, NSW 2007, Australia. Lan.Wu-2@uts.edu.au This work was supported by ARIA Research and the Australian Government via the Department of Industry, Science, and Resources CRC-P program (CRCPXI000007) and the Australian Research Council Discovery Project under Grant DP210101336.

This work has been submitted to the IEEE for possible publication. Copyright may be transferred without notice, after which this version may no longer be accessible.

<sup>3</sup>[https://github.com/UTS-RI/VDB\\_GPFD](https://github.com/UTS-RI/VDB_GPFD)

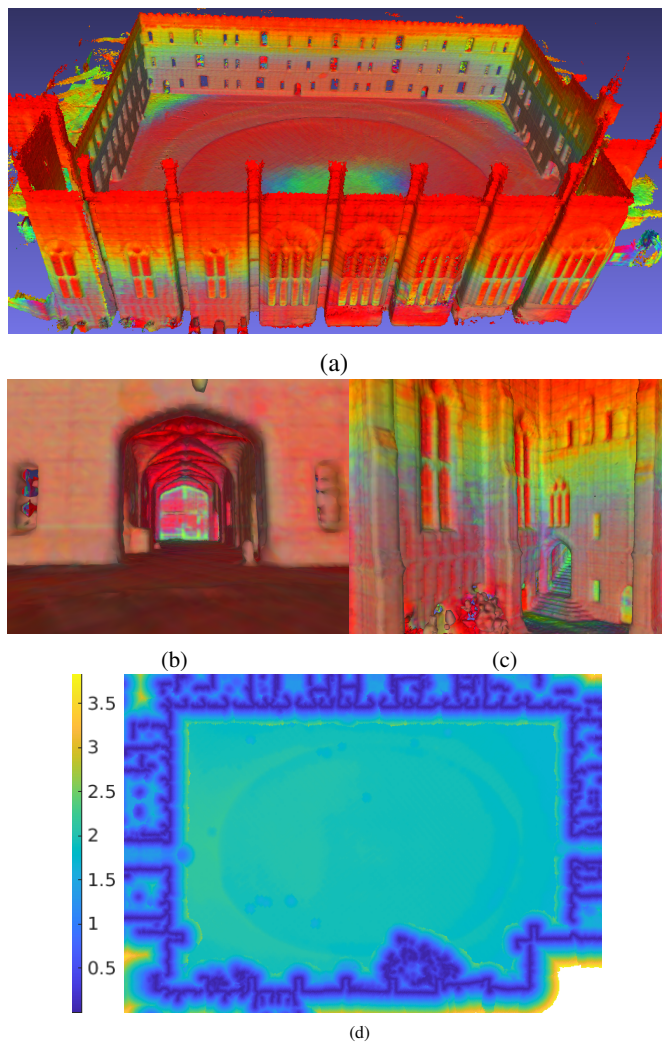


Fig. 1: 3D dense reconstruction and distance field from VDB-GPDF framework. a) Shows the incrementally built mesh coloured with the fused LiDAR intensity. Zooming in to visualise b) the ceiling inside the corridor and c) the stairs and windows around the corner of the quad. d) Shows a horizontal slice of the inferred distance field 0.9m above the ground.

Recent frameworks based on distance field representations that fulfil some of the above-mentioned requirements have been proposed in the robotics literature [1], [2], [3], [4], [5]. In general, these frameworks are dense and efficient enough to run online, can deal up to a certain point with dynamic objects and are catered to any depth sensor. Most of them incrementally build a projective [1], [3] or non-projective [5] Truncated Signed Distance Field (TSDF) or occupancy map [2], [4] and some can then recover an approximation of the Euclidean Signed Distance Field (ESDF) [1], [2], [5], [4]. Despite being

dense volumetric representations, these frameworks do not rely on generative models thus the representation is maintained at the resolution that was built and only contains information where the data was observed.

On the other hand, Gaussian Process (GP)-based framework proposed in our previous work [6], [7], [8] are probabilistic generative models that are capable of building accurate Euclidean Distance Field (EDF)s. GP-based frameworks, however, suffer from high computational complexity. To solve this issue and allow online incremental mapping works like [9], [8], [10] use the Octree data structure. The time of accessing the Octree grows with the number of nodes, thus suffering from scalability issues for large datasets. As a fast-access data structure, OpenVDB was used recently proposed in VDBFusion [3]. VDBFusion is a very efficient incremental reconstruction framework based on TSDF, which does not recover the EDF.

In this paper, we propose a framework that couples the OpenVDB data structure with GP distance fields. The so-called VDB-GPDF framework builds a scene representation that aims to meet all the key requirements mentioned above. It offers the accuracy and scalability to build a global and incremental scene representation that can cater for room-sized indoor scenes and large-scale outdoor datasets and is compatible with depth sensing such as RGB-D cameras or LiDARs. VDB-GPDF deals implicitly with dynamic changes, handles probabilistically noisy measurements, and has the ability to complete data at the required resolution. Our framework can provide multiple outputs such as accurate Euclidean distance, its gradients, surface properties like colour, intensity or instance segmentation, and a dense mesh with informative textures. The key aspect of this work is the local VDB structure that contains a Local GP Signed Distance Field (L-GPDF), a temporary latent model that enables queries at arbitrary testing points on the current field of view. Followed by a probabilistic fusion that merges the inferred values of the testing points into a global VDB. The contributions of this paper are as follows:

- A seamless coupling of the GPDF with VDB data structure to enable online incremental performance for large-scale mapping.
- A probabilistic fusion that given the current measurements fits a local GPDF, which allows us to fuse using its mean and uncertainty with the global ESDF and other surface properties.
- A generative model that efficiently produces the ESDF via a Global GPDF trained based on the estimated surface which enables downstream applications to query accurate distance and gradients.

We evaluate our proposed VDB-GPDF against the state-of-the-art frameworks showing comparable reconstruction performance and superior efficiency and accuracy of the inferred distance field.

## II. RELATED WORK

Efficient dense volumetric mapping is appealing for the ability to incrementally build a representation of an unseen environment that can be used for localisation, visualisation, navigation and manipulation in particular when the output space

is an ESDF. Inspired by [11], frameworks like Voxblox [1] and Voxfield [12] propose solutions to compute the ESDF as a post-processing step from the projective or non-projective TSDF respectively through wavefront propagation using BFS (Breadth-First Search) algorithm. Using occupancy instead of TSDF, FIESTA [2] also obtains the ESDF from the very efficiently built occupancy map using multiple customised data structures. Employing a less customised data structure, VDB-EDT adopts OpenVDB [13], [14] for occupancy mapping and a distance transform function to represent the EDF hierarchically [4]. Other than occupancy mapping, VDBFusion [3] combines OpenVDB with TSDF fusion to generate volumetric dense maps efficiently. However, VDBFusion does not generate the ESDF as an output. VDBblox [5] adopts the OpenVDB structure to maintain high efficiency. However, VDBblox continues to use TSDF fusion and then propagates it to approximate the ESDF as in [12].

Instead of TSDF or occupancy fusion as all these approaches, we propose to fuse directly on ESDF using an L-GPDF, which allows us to query the Euclidean distance with uncertainty for any point in the field of view. The fusion is then done by merging the inferred ESDF values into the global OpenVDB structure. In Table I, we summarise the most popular online dense volumetric mapping frameworks and add the proposed framework to highlight its difference and novelty.

GP-based distance fields have been proposed as a probabilistic and generative model to represent complex environments [9], [6]. In our prior work [6], [7], we proposed a theoretical sound formulation to estimate the Euclidean distance field by applying the logarithmic transformation to a GP formulation. To improve the accuracy of the distance estimate, we later introduced the reverting GP distance field [8]. Although GP-based frameworks are computationally intensive, Octree structures have enabled fast computations in [9], [8] and more recently in [10] for online incremental mapping. However, Octrees expand the nodes overtime and require tree traversal resulting in a less scalable data structure for large scenarios. Recently, methods like the Gaussian surface model or mixture model [15] have been introduced to model an EDF using fused point clouds or batch mapping, but a substantial gap remains in achieving incremental performance. Via the VDB data structure, our proposed approach facilitates efficiency and scalability while maintaining the advantages of the GPDFs.

Beyond GPs, other generative methods for dense volumetric mapping have recently been proposed in the literature. A large

TABLE I: Comparison of online dense mapping frameworks

Framework	Data Structure	Fusion	Mesh	ESDF
VDBFusion [3]	OpenVDB	TSDF	✓	✗
VDB-EDT [4]	OpenVDB	Occupancy	✗	✓
VDBblox [5]	OpenVDB	TSDF	✓	✓
Voxblox [1]	Hash Map	TSDF	✓	✓
Voxfield [12]	Hash Map	TSDF	✓	✓
FIESTA [2]	Multiple	Occupancy	✗	✓
VDB-GPDF (ours)	OpenVDB	ESDF	✓	✓

number of works have examined the potential of deep learning techniques for EDF representations. Inspired by [16], the work in [17] proposes using an implicit neural representation with Eikonal regularisation to approximate the ESDF for points distant from the surface. The work in [18] introduced learning an EDF approximation from Neural Radiance Fields (NeRFs) using occupancy. Similarly, inspired from [17], iSDF [19] is proposed to use a neural signed distance field for mapping. To achieve efficient performance in the learning approach, DI-Fusion [20] proposes an online incremental SDF using clustering blocks, and HIO-SDF [21] applies hierarchical data structure. Despite the advantages of this type of continuous representation with low memory consumption, all these approaches need extensive pre-training to enable incremental mapping and rely on high-performance GPU capabilities.

### III. PRELIMINARIES

#### A. Gaussian Process Distance Field

GP [22] is a non-parametric regression approach that models a distribution over functions. We use the so-called GP Distance Field method originally presented in [8] to model our distance field. Consider a surface  $S$  in a Euclidean space  $\mathbb{R}^D$ , and a set of discrete observations of  $S$  as  $\mathbf{y} = \{y_j\}_{j=1}^J \in \mathbb{R}$  taken at locations  $\mathbf{X} = \{\mathbf{x}_j\}_{j=1}^J \in \mathbb{R}^D$ . By modelling the latent scalar field which can be interpreted as an occupancy field  $o(\mathbf{x}) : \mathbb{R}^D \mapsto \mathbb{R}$  of the space with a GP as  $o \sim \mathcal{GP}(0, k(\mathbf{x}, \mathbf{x}'))$ , it is possible to infer  $\hat{o}(\mathbf{x}_*)$  at any location in the space. Let us arbitrarily define the occupied area to be equal to 1. Therefore,  $y$  is equal to  $\mathbf{1}$  for the GP latent inference

$$\hat{o}(\mathbf{x}_*) = \mathbf{k}_{\mathbf{x}_* \mathbf{X}} (\mathbf{K}_{\mathbf{X}\mathbf{X}} + \sigma_o^2 \mathbf{I})^{-1} \mathbf{1}. \quad (1)$$

where  $\sigma_o^2$  is the variance of noise. The uncertainty is then inferred using

$$\hat{u}(\mathbf{x}_*) = \mathbf{k}_{\mathbf{x}_* \mathbf{x}_*} + \mathbf{k}_{\mathbf{x}_* \mathbf{X}} (\mathbf{K}_{\mathbf{X}\mathbf{X}} + \sigma_o^2 \mathbf{I})^{-1} \mathbf{k}_{\mathbf{X}\mathbf{x}_*}. \quad (2)$$

The distance field  $\hat{d}(\mathbf{x}_*)$  given any location  $\mathbf{x}_*$  is obtained by applying the *reverting* function  $r$  to the latent field as

$$\hat{d}(\mathbf{x}_*) = r(\hat{o}(\mathbf{x}_*)). \quad (3)$$

Considering the square exponential kernel  $k(\mathbf{x}, \mathbf{x}') = \sigma^2 \exp\left(-\frac{\|\mathbf{x} - \mathbf{x}'\|^2}{2l^2}\right)$ , substituting the reverting function of square exponential kernel into Eq. 3 gives us the distance inference at  $\mathbf{x}_*$ ,

$$\hat{d}(\mathbf{x}_*) = \sqrt{-2l^2 \log\left(\frac{\hat{o}(\mathbf{x}_*)}{\sigma^2}\right)}. \quad (4)$$

and variance as

$$\hat{v}(\mathbf{x}_*) = \Lambda \hat{u}(\mathbf{x}_*) \Lambda^\top. \quad (5)$$

where  $\Lambda$  is equal to  $l\sigma_o^2/(\hat{o}(\mathbf{x}_*) \sqrt{2 \log(\hat{o}(\mathbf{x}_*)/\sigma_o^2)})$ . As pointed out in [8], the variance of the latent field is propagated through the reverting function using its Jacobian with the linearisation point at the surface. Faraway from the surface, the uncertainty of the estimated distance field grows rapidly. Therefore, the variance is only informative around the surface.

Furthermore, to estimate the gradient of the distance field, we simply apply the differentiation (linear) operator as

$$\nabla \hat{d}(\mathbf{x}_*) = \nabla \mathbf{k}_{\mathbf{x}_* \mathbf{X}} (\mathbf{K}_{\mathbf{X}\mathbf{X}} + \sigma_o^2 \mathbf{I})^{-1} \mathbf{1}, \quad (6)$$

where  $\nabla \mathbf{k}_{\mathbf{x}_* \mathbf{X}}$  is the partial derivative of the kernel matrix with respect to  $\mathbf{x}$ .

#### B. OpenVDB Data Structure

The commonly used Octree data structure [9] usually divides the full scene into spatial clusters in a multi-layer tree and treats each cluster separately. However, as the scene grows, the Octree expands with more nodes, and tree traversing gets slower as the access complexity  $\mathcal{O}(\log n)$  is related to the number of nodes  $n$ . OpenVDB data structure (Volumetric, Dynamic grid that shares several characteristics with B+trees) [14], [13] is used in this work to enable efficient, large-scale, dense incremental mapping. This hierarchical tree-like structure allows us to efficiently divide GP into clusters with constant computational complexity to access them.

The B-tree-like three-dimensional VDB data structure comprises sparse collections of voxel blocks in four layers: root nodes, leaf nodes, and usually two levels of internal nodes. The default configuration is typical  $2^3 \times 2^3 \times 2^3$  voxels in each leaf node,  $2^4 \times 2^4 \times 2^4$  of leaf nodes in a first-layer of internal node, and  $2^5 \times 2^5 \times 2^5$  of the first-layer of internal nodes in a second-layer of internal node. Therefore, a second-layer of internal node subsumes a three-dimensional block of voxels of size  $4096 \times 4096 \times 4096$ . Unlike the internal nodes and leaf nodes, the number of children of the root node is not explicitly fixed. As default, each root node has 4 second-layer internal nodes. This hierarchical tree structure is fixed with four height layers across the involved tree, maintaining a shallow and broad representation compared to octrees. The constant height of the VDB tree allows constant and fast traversing from the root node to the leaf node. Any random access can operate at a consistent computational complexity in average  $\mathcal{O}(1)$ . Furthermore, VDB substantially reduces contemporary CPU memory consumption by hierarchically allocating the nodes even with extreme grid resolution.

The memory and time efficiency properties of VDB [13] are highly suitable for our online mapping frameworks. Note that each leaf node in VDB is a proper-sized GP cluster, and we use the leaf iterator to traverse available voxels in each leaf node and then use them to train each GP cluster separately.

### IV. VDB-GPDF FRAMEWORK

To incrementally build and maintain a persistent, efficient, large-scale, adaptable, robust and dense distance field map of the environment with depth sensors, we propose to couple GPDF [8] with local and global VDB data structures. Fig. 2 shows the diagram of our proposed VDB-GPDF framework.

Depth sensor data is captured as a raw point cloud  ${}^{C_i} \mathcal{P}_{\{i\}}$  in sensor frame  $C_i$  at current time  $i$ . The estimated pose is used to project the point cloud from current sensor frame  $C_i$  to world frame  $W$  given the homogeneous transformation matrix  $\mathbf{T}_{C_i}$  yielding a point cloud  $\mathcal{P}_{\{i\}}$  in the world reference frame. The raw points  $\mathcal{P}_{\{i\}}$  are voxelised into the voxels denoted as  $\mathcal{P}_{v\{i\}}$

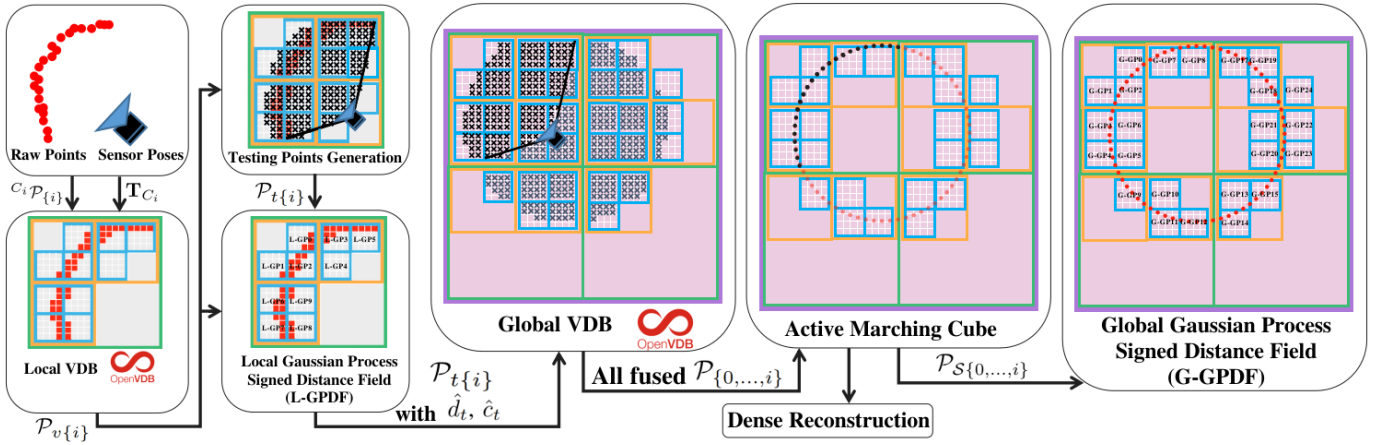


Fig. 2: Block Diagram of the proposed VDB-GPDF framework. We first model the temporary Local Gaussian Process Signed Distance Field (L-GPDF) and surface properties using  $\mathcal{P}_{v\{i\}}$ . A set of testing points along the ray from the sensor origin to  $\mathcal{P}_{v\{i\}}$  are generated to query the distance and surface properties inferences of L-GPDF. Each point in  $\mathcal{P}_{t\{i\}}$  with its inferred  $\hat{d}_t$  and  $\hat{c}_t$  are fused with the full map represented by a global VDB. Then we have all fused voxels  $\mathcal{P}_{\{0,\dots,i\}}$ . The marching cube is applied on the active voxels in  $\mathcal{P}_{\{0,\dots,i\}}$  to update the zero crossing points  $\mathcal{P}_{S\{0,\dots,i\}}$  and dense reconstruction. The global Gaussian Process Signed Distance Field (G-GPDF) is modelled by  $\mathcal{P}_{S\{0,\dots,i\}}$  in each leaf node in the global VDB separately.

via a local hierarchical VDB. Thus,  $\mathcal{P}_{v\{i\}}$  is divided into local clusters maintained by the VDB leaf nodes. For each leaf node, the centres of voxels are used as training points to model GPs separately for distance and surface properties. All GPs together form the temporary Local Gaussian Process Signed Distance Field (L-GPDF) along with surface properties. In addition,  $\mathcal{P}_{v\{i\}}$  is passed to the testing points generation block. A ray-cast operation from the current sensor origin to each voxel in  $\mathcal{P}_{v\{i\}}$  is performed to generate a set of voxels. These voxels are then used as the testing points  $\mathcal{P}_{t\{i\}}$  to query the L-GPDF. Let us denote each point in  $\mathcal{P}_{t\{i\}}$  as  $\mathbf{x}_*$ . Note that the distance sign of each  $\mathbf{x}_*$  is computed given the sensor origin and  $\mathcal{P}_{v\{i\}}$ . For each querying point  $\mathbf{x}_*$ , the closest node in L-GPDF is found to compute the GP distance inference  $\hat{d}_t(\mathbf{x}_*)$ , surface properties  $\hat{c}_t(\mathbf{x}_*)$  and uncertainty.

The  $\hat{d}_t$  and  $\hat{c}_t$  estimates (mean and uncertainty) at each location in  $\mathcal{P}_{t\{i\}}$  are then fused with the existing map maintained by a global VDB grid, which has all fused voxels  $\mathcal{P}_{\{0,\dots,i\}}$ . The leaf nodes in the global VDB grid that participated in the fusion procedure are marked as active. Marching cubes algorithm [23] is then performed for the voxels in the active nodes to recover the dense reconstruction. The zero crossing points  $\mathcal{P}_{S\{0,\dots,i\}}$  in active nodes and previous active nodes are used to generate the global Gaussian Process Signed Distance Field (G-GPDF). Similar to L-GPDF, each leaf node is trained separately. The G-GPDF is available to be queried for any given point in the set of all points the space  $\mathcal{P}_o$  of downstream applications that require accurate distance  $\hat{d}_o$  and gradients  $\nabla \hat{d}_o$ , e.g., navigation, path planning, localisation and manipulation.

#### A. Local Gaussian Process Signed Distance Field

We propose to efficiently voxelise the raw points  $\mathcal{P}_{\{i\}}$  in the world frame into a set of voxels via a local hierarchical VDB. The method groups all raw points projecting into the same voxel. Therefore, a dense raw point cloud  $\mathcal{P}_{\{i\}}$  is represented

by the centres of voxels, denoting as  $\mathcal{P}_{v\{i\}}$ . We simply perform the further fusion and integration once for each voxel. Taking advantage of efficient access to VDB, the voxelisation procedure is fast and  $\mathcal{P}_{v\{i\}}$  is automatically divided into leaf nodes maintained by the VDB.

We iterate each leaf node of the local VDB for voxels, which are used as training points to formulate each node as a GP separately. All GPs in local VDB consist of the temporary Local Gaussian Process Signed Distance Field (L-GPDF) along with surface properties. As explained in Section. III-A, given locations of voxels, we compute the distance field inference and variance via Eq. 4 and Eq. 5. In addition, given the voxels' surface properties of each leaf node, we propose to model the surface properties inference:

$$\hat{c}_t(\mathbf{x}_*) = \mathbf{k}_{\mathbf{x}_*} \mathbf{x} (\mathbf{K}_{\mathbf{X}\mathbf{X}} + \sigma_c^2 \mathbf{I})^{-1} \mathbf{c}. \quad (7)$$

Therefore, L-GPDF is ready for the testing points to query the distance, surface properties and variance. Note that the temporary and local L-GPDF is re-modelled at every frame  $i$ .

#### B. Testing Points Generation

Testing points generation method takes  $\mathcal{P}_{v\{i\}}$  and sensor origin as input. Here, we adopt a similar idea as the so-called free space carving method [1], [3] to update the distance information for the voxels within the current sensor field of view. Free-space carving has the ability to update the dynamically changing objects in the scene. We propose three main improvements to enhance efficiency while achieving comparable reconstruction results to the conventional free-space carving used in most volumetric mapping methods.

First, we propose a voxelisation method to ray-cast from the current sensor origin to each voxel in  $\mathcal{P}_{v\{i\}}$ . This results in a faster traverse than ray-casting for each raw point cloud  $\mathcal{P}_{\{i\}}$  and produces comparable zero crossing. Secondly, the naive ray-casting usually iterates and updates all voxels intersected by the ray in order. This may lead to updating the

voxel without any surface measurement or the same voxel multiple times due to having different ray intersections. In contrast, we only query the voxel, which has previous surface measurements in the field of view. In this way, the existence of the previous surface is updated. Therefore, the dynamic objects are handled implicitly and efficiently. Note that testing all points in the frustum is time-consuming and not necessary in our framework. Despite we can get the fused ESDF this does not produce a generative model that can be queried anywhere in the space. Therefore, we choose to infer only the relevant testing points for fusion, making this process more efficient and later generating the accurate ESDF using G-GPDF as explained in the next section. Thirdly, we compute the surface normals given  $\mathcal{P}_{v\{i\}}$  and generate voxels along the normal direction up to a certain distance even outside the frustum. When the sensor ray is close to being parallel to the observed surface, the naive ray-casting cannot generate enough testing voxels around the surface. Having extra voxels along the normal direction yields a complete reconstruction.

We use  $\mathcal{P}_{t\{i\}}$  to query the distance through the L-GPDF. For each  $\mathbf{x}_*$  in  $\mathcal{P}_{t\{i\}}$ , we find the closest node in L-GPDF and use the node GP to compute the GP distance inference  $\hat{d}_t(\mathbf{x}_*)$ , surface property inference  $\hat{c}_t(\mathbf{x}_*)$ , and variances  $\hat{v}_t(\mathbf{x}_*)$  and  $\hat{w}_t(\mathbf{x}_*)$ . Thanks to the available Euclidean distance inference of L-GPDF, we only query each voxel once to perform the fusion later. This leads to a comparable result of the final reconstruction but more efficiently than TSDF fusion. Note that we also compute the sign of distance given the sensor origin and  $\mathcal{P}_{v\{i\}}$ .

### C. Data Fusion

After querying the testing points from the L-GPDF, we have the signed distance inference  $\hat{d}_t(\mathbf{x}_*)$ ,  $\hat{c}_t(\mathbf{x}_*)$  and variance  $\hat{v}_t(\mathbf{x}_*)$   $\hat{w}_t(\mathbf{x}_*)$  for each  $\mathbf{x}_*$  in  $\mathcal{P}_{t\{i\}}$ . Unlike the commonly used TSDF fusion that uses constant or drop-off weights to fuse the projective (or non-projective) distance, we directly query our probabilistic L-GPDF to fuse the distance and surface properties through its mean and variance in the global VDB. Note that the fusion is mostly done around the surface, as our variance is only accurate near the surface, as discussed in Section III.

The global VDB efficiently accesses the previous distance mean and weight at  $\mathbf{x}_* \in \mathcal{P}_{t\{i\}}$ , which are denoted as  $D_{i-1}(\mathbf{x}_*)$  and  $V_{i-1}(\mathbf{x}_*)$  respectively. Then  $D_i(\mathbf{x}_*)$  and  $V_i(\mathbf{x}_*)$  is estimated given the new queried  $\hat{d}_t(\mathbf{x}_*)$   $\hat{v}_t(\mathbf{x}_*)$  of L-GPDF. We then perform the distance fusion following the standard weighted sum as in [24],

$$\begin{aligned} D_i(\mathbf{x}_*) &= \frac{V_{i-1}(\mathbf{x}_*) \cdot D_{i-1}(\mathbf{x}_*) + (1 - \hat{v}_t(\mathbf{x}_*)) \cdot \hat{d}_t(\mathbf{x}_*)}{V_{i-1}(\mathbf{x}_*) + (1 - \hat{v}_t(\mathbf{x}_*))} \\ V_i(\mathbf{x}_*) &= V_{i-1}(\mathbf{x}_*) + (1 - \hat{v}_t(\mathbf{x}_*)). \end{aligned} \quad (8)$$

Similarly, the surface properties are fused using

$$\begin{aligned} C_i(\mathbf{x}_*) &= \frac{W_{i-1}(\mathbf{x}_*) \cdot C_{i-1}(\mathbf{x}_*) + (1 - \hat{w}_t(\mathbf{x}_*)) \cdot \hat{c}_t(\mathbf{x}_*)}{W_{i-1}(\mathbf{x}_*) + (1 - \hat{w}_t(\mathbf{x}_*))} \\ W_i(\mathbf{x}_*) &= W_{i-1}(\mathbf{x}_*) + (1 - \hat{w}_t(\mathbf{x}_*)). \end{aligned} \quad (9)$$

### D. Global Gaussian Process Signed Distance Field

After the fusion process, the leaf nodes in the global VDB grid are marked as active nodes. We perform the marching cubes for the voxels of active nodes and for computing the dense reconstruction with surface properties. The zero crossing points in current active nodes  $\mathcal{P}_{S\{i\}}$  then merge into  $\mathcal{P}_{S\{0,\dots,i\}}$ . Zero crossing points in each node are used to train separate GPs. The combination of all GPs forms the global Gaussian Process Signed Distance Field (G-GPDF).

Note that when querying the G-GPDF, we only search for a certain number of closest nodes through a kd-tree for each querying point and only perform the corresponding GP training and inference for these nodes. In this way, we avoid training unnecessary GP nodes which no points are querying them. This will avoid redundancy in computing the GP of the entire field. In addition, we use the smooth minimum function for the distance field to ensure accurate global consistency.

When partitioning the full map into leaf nodes in the VDB data structure, modelling the clustering GP of each node suffers from discontinuity around the boundaries. A common solution is to have overlapping parts with neighbouring nodes. However, this method extends the volume of each node therefore the GP training becomes more complex in terms of computations. Instead, we address the problem by using the smooth minimum function to estimate the continuous distance field. We search for the number of  $Q$  clustered GP nodes in the map and recover the distance as,

$$\hat{d}(\mathbf{x}_*) = \frac{\sum_{q=1}^Q \hat{d}_q(\mathbf{x}_*) \exp(\lambda \hat{d}_q(\mathbf{x}_*))}{\sum_{q=1}^Q \exp(\lambda \hat{d}_q(\mathbf{x}_*))}, \quad (10)$$

where  $\lambda$  is a large positive value to control the evenness of the smooth minimum. We use 100 for  $\lambda$  in this paper.  $\hat{d}_q(\mathbf{x}_*)$  is the distance inference at querying location  $\mathbf{x}_*$  given the located GP node with the index of  $q$ . For the gradient, we directly average the inferred gradients from the  $Q$  clustered GP nodes.

## V. EVALUATION

To evaluate the proposed VDB-GPDF framework, we quantitatively compare the mapping performance for a) efficiency, b) reconstruction accuracy and c) distance accuracy, and qualitatively demonstrate the mapping performance for a room size with RGB-D cameras and a LiDAR large-scale dataset. Our framework is implemented in C++ based on ROS1. All experiments were run on 12th Gen Intel® Core™ i5-1245U with 12 cores.

The first dataset is the Cow and Lady<sup>1</sup>, which includes fibre-glass models of a large cow and a lady standing side by side in a room. The dataset consists of RGB-D point clouds collected using a Kinect 1 camera, with sensor trajectory captured using a Vicon motion system. We use frames 220-820 of the dataset, which covers major information of the scene. For the second dataset, we choose the Newer College dataset [25] collected by a handheld sensor platform with a 128-beam ouster LiDAR.

<sup>1</sup><https://projects.asl.ethz.ch/datasets/doku.php?id=iros2017>

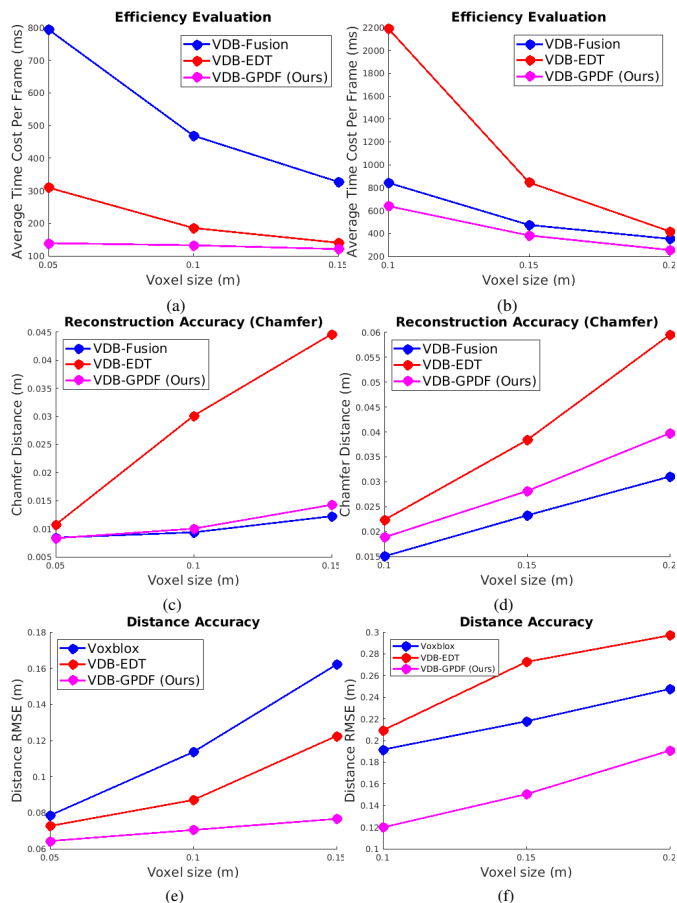


Fig. 3: Quantitative comparisons of a) and b) the efficiency performance, c) and d) reconstruction accuracy in Chamfer distance, e) and f) the distance field accuracy on the cow and lady RGB-D dataset and the newer college LiDAR dataset.

The estimated poses are calculated via the alignment of each frame to the ground truth map. The size of the main quad is roughly  $56 \times 40 \times 20$  m, with approximately 2000 frames. Both Cow and Lady and Newer College have the ground truth map that allows us to perform a proper quantitative evaluation for both reconstruction and distance field accuracy. For a fair comparison, we process every frame from both datasets in each framework. Our strategy for length scale selection depends on the number of voxels in each leaf node, which in our case is fixed to  $2^3 \times 2^3 \times 2^3$  voxels. A length scale that correlates two to four voxels is a good trade-off between smoothing and interpolation for our kernel function.

### A. Fusion Performance

First, we want to evaluate the proposed fusion. We compare the proposed ESDF fusion with TSDF fusion in VDBFusion. For the sake of fairness, we apply the same voxelisation method in Sec. IV-B for VDBFusion as in our proposed method. A qualitative comparison of the TSDF fusion of VDBFusion and the proposed ESDF fusion with full testing voxels in the frustum is demonstrated in Fig. 4a and 4b. The white boxes are the measurements, and the coloured flat squares are the inferred distance values of testing points for fusion in the field of view. The results show that our ESDF

fusion produces accurate and natural inferred distance of each point in the frustum. After performing the fusion for all frames, we compare the reconstructed mesh for TSDF fusion and our fusion. Our reconstruction in 4d shows less noise in the wall, more complete on the mattress and cow legs than 4c, lower reconstruction error in Chamfer distance.

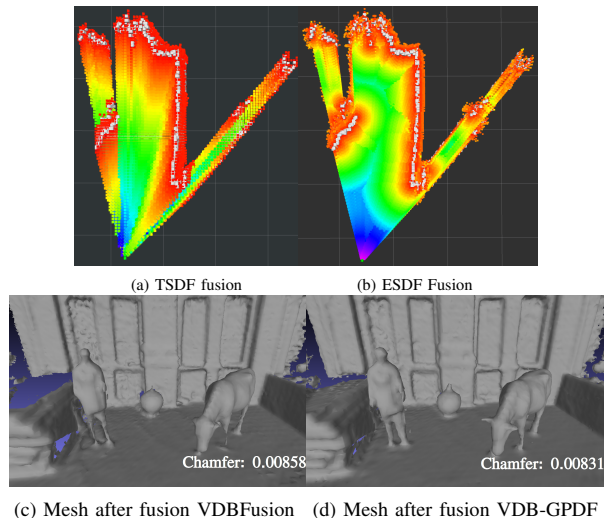


Fig. 4: Qualitative and quantitative comparison of a) the TSDF fusion from VDBFusion and b) our proposed ESDF fusion with full testing points in the frustum. b) shows that our approach reasons directly in the Euclidean space. After the fusion, our reconstruction in d) shows less noise in the wall and is more complete on the mattress and cow legs than c).

### B. Efficiency

We first evaluate the VDB-GPDF efficiency against the state-of-the-art mapping frameworks VDB-Fusion and VDB-EDT, both developed based on OpenVDB data structure. Fig. 3a and 3b show the average computational time per frame for the room size RGB-D Cow and Lady dataset and the outdoor LiDAR Newer College dataset, respectively. Note that the Newer College quad has pedestrians walking by as dynamic objects. Both frameworks have free-space carving methods enabled to update the moving objects in the scene. For the sake of simplicity, we compute the average time for all the integration processes, including fusion and ESDF. As for our framework, we include L-GPDF, incremental fusion and G-GPDF. Both figures show that our VDB-GPDF is more efficient than other frameworks with varying resolutions due to our voxelisation method and fewer testing points in the frustum area. VDBFusion consumes more time in the RGB-D dataset than others due to enabling the free-space carving process. For the LiDAR data, VDB-EDT requires more time to update the EDF every frame.

### C. Reconstruction Accuracy

VDBFusion and VDB-GPDF both produce similar meshes of the scene shown in Fig. 5a and Fig. 5b, respectively. VDB-GPDF produces a more complete and natural reconstruction, especially when the sensor is parallel to the observed surface.

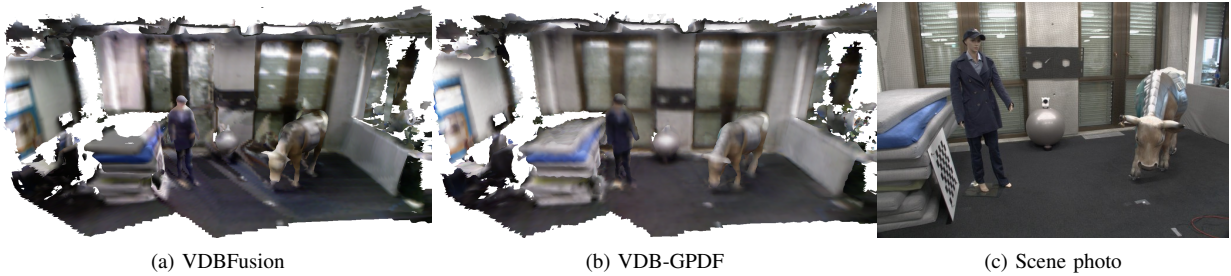


Fig. 5: Qualitative reconstruction comparison of a) VDBFusion and b) our proposed method shows that VDB-GPDF produces a more complete and natural reconstruction, especially when the sensor is in parallel with the observed surface. Our mesh covers on the top of the mattress, and the colour is properly fused for visualisation as the scene photo colour in c).

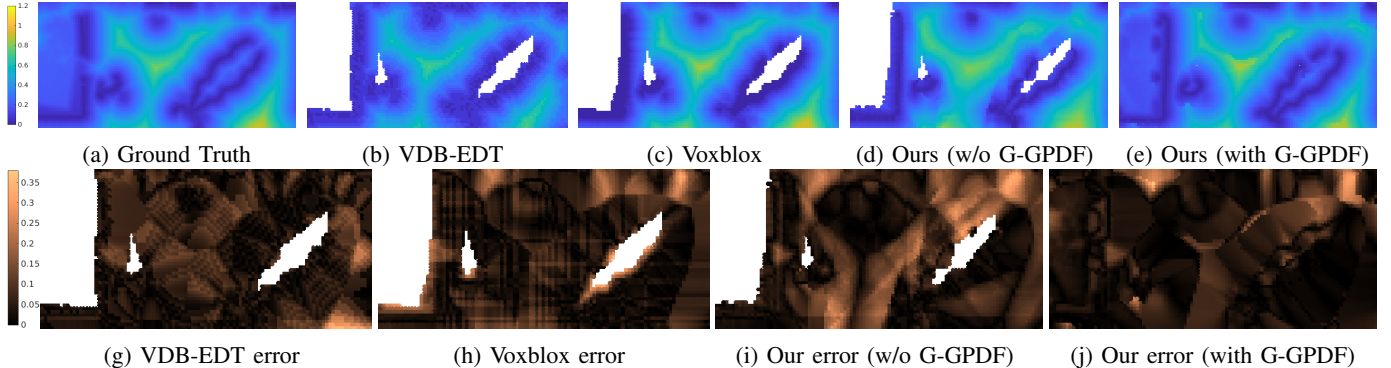


Fig. 6: Comparison of ground truth and estimated EDF with a 2D horizontal slice 0.9 m above the ground for the Cow and Lady dataset. The resolution is 0.05m. e) is accurate and closely resembles the ground truth in a). b). c) and d) do not produce enough smoothness in the field and only offer values in the observed area. Our VDB-GPDF with G-GPDF in j) produces lower and smoother values of distance errors than VDB-EDT in g) and Voxblox in h) and our method without the G-GPDF in i).

It can be seen that there is a gap at the top of the mattresses on the left-hand side in the VDBFusion result, whereas VDB-GPDF does not have the same gap. In addition, our colour is nicely fused with a sample of the RGB camera data in c) for qualitative comparison. Note that, for example, around the wall and floor, our method shows the colour with high fidelity, while VDBFusion colour is more approximate.

We use the Chamfer distance metrics [26] against VDB-Fusion and VDB-EDT to compare the maps on both datasets quantitatively. As demonstrated in Fig. 3c and 3d, our map quality outperforms VDB-EDT in different resolutions. Due to our voxelisation method being applied, we have comparable results to VDBFusion in reconstruction accuracy. To show the performance in a large-scale dataset, we use the main quad of the Newer College, which is roughly  $56 \times 40 \times 20$  m, with approximately 2000 frames in the dataset. In Fig. 1, we qualitatively show our mesh coloured by fused LiDAR intensity and the distance field output. Fig. 1a shows the incrementally built dense reconstruction. We zoomed in Fig. 1b to show the textures on the ceiling inside the corridor and Fig. 1c the stairs and windows at the corner of the quad.

#### D. Distance Accuracy

We evaluate the proposed GP distance field with VDB structure against Voxblox and VDB-EDT since the VDBFusion framework has no EDF. We use the ground truth point cloud to compute the distance field ground truth numerically. We compute the distance field on a regular 3D grid of 5cm

resolution for the RGB-D case and 10 cm for the LiDAR case. The RMSE error given the ground truth distance field is shown in Fig. 3e and 3f. Our distance field has the most accurate results. Voxblox produces the large distance RMSE for the RGB-D dataset, and VDB-EDT has a larger error on the Newer College dataset than others due to failure to clear the moving objects successfully.

To further examine the behaviour of VDB-GPDF, we compare 2D slices of the ground-truth and estimated distance fields in Fig. 6. We choose a horizontal slice 0.9m above the ground, roughly cutting the scene objects in the middle. In addition, we evaluate the EDF with and without the G-GPDF enabled to show that G-GPDF produces more accurate distance inference than fusing the ESDF directly. Moreover, G-GPDF is a generative model that can generate distance and gradient inference even in places with no observations. As shown in Fig. 6b, 6c and Fig. 6d, VDB-EDT and Voxblox and VDB-GPDF without G-GPDF only compute the EDF within the sensor’s field of view, whereas VDB-GPDF with G-GPDF naturally predicts the EDF value at all points as can be seen in Fig. 6e. For a quantitative evaluation, we illustrate the distance error with a colour map in Fig. 6g, 6h, 6i and 6j. Our VDB-GPDF produces lower and smoother values of distance errors.

Similarly, for the LiDAR dataset, we compare 2D slices of the ground-truth and estimated distance fields in Fig. 7. As shown in Fig. 7b, 7c and 7d, our VDB-GPDF computes the similar EDF as the ground truth in Fig. 7a. For a quantitative evaluation, we plot the same distance absolute error in Fig. 6g, 6h and 6j. Our VDB-GPDF generates lower and more

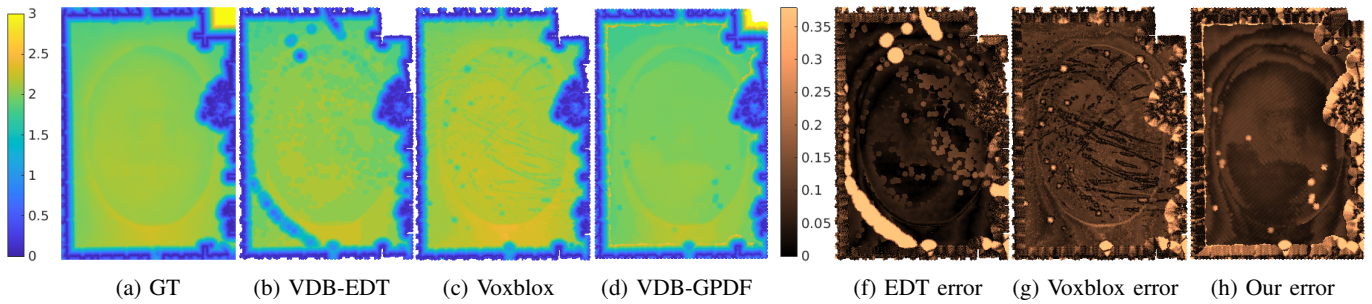


Fig. 7: Comparison of ground truth and estimated EDF with a 2D horizontal slice 0.9 m above the ground for the newer college. d) is accurate and closely resembles the ground truth in a). b) fails to update in the areas where moving objects are present. c) does not produce enough smoothness in the field. Similarly, Our VDB-GPDF in h) produces lower and smoother values of distance errors than VDB-EDT in f) and Voxblox in g) with the LiDAR dataset.

consistent distance error values.

## VI. CONCLUSION

We propose VDB-GPDF, a framework that couples VDB structure and GPDF for online incremental mapping. It has the scalability to build a large-scale scene representation and is compatible with different types of depth sensors. It offers a comparable reconstruction of the scene environment and accurate Euclidean distance against state-of-the-art approaches. VDB-GPDF can implicitly adapt to dynamic changes and probabilistically handle noisy measurements. VDB-GPDF provides flexible multiple outputs such as Euclidean distance and gradient fields, surface properties including colour and intensity, and a dense mesh with informative textures. Future work considers unlocking the ability to predict motion using the efficiently built changing distance field.

## REFERENCES

- [1] H. Oleynikova, Z. Taylor, M. Fehr, R. Siegwart, and J. Nieto, "Voxblox: Incremental 3D Euclidean Signed Distance Fields for on-board MAV planning," in *2017 IEEE/RSJ International Conference on Intelligent Robots and Systems (IROS)*. IEEE, Sep. 2017.
- [2] L. Han, F. Gao, B. Zhou, and S. Shen, "FIESTA: Fast Incremental Euclidean Distance Fields for Online Motion Planning of Aerial Robots," 2019.
- [3] I. Vizzo, T. Guadagnino, J. Behley, and C. Stachniss, "Vdbfusion: Flexible and efficient tsdf integration of range sensor data," *Sensors*, vol. 22, no. 3, p. 1296, 2022.
- [4] D. Zhu, C. Wang, W. Wang, R. Garg, S. Scherer, and M. Q.-H. Meng, "VDB-EDT: An Efficient Euclidean Distance Transform Algorithm Based on VDB Data Structure," May 2021. [Online]. Available: <https://arxiv.org/abs/2105.04419v1>
- [5] Y. Bai, Z. Miao, X. Wang, Y. Liu, H. Wang, and Y. Wang, "Vdbblox: Accurate and efficient distance fields for path planning and mesh reconstruction," in *2023 IEEE/RSJ International Conference on Intelligent Robots and Systems (IROS)*. IEEE, 2023, pp. 7187–7194.
- [6] L. Wu, K. M. B. Lee, L. Liu, and T. Vidal-Calleja, "Faithful Euclidean Distance Field from Log-Gaussian Process Implicit Surfaces," Jan. 2021, arXiv:2010.11487 [cs]. [Online]. Available: <http://arxiv.org/abs/2010.11487>
- [7] L. Wu, K. M. B. Lee, C. Le Gentil, and T. Vidal-Calleja, "Log-GPIS-MOP: A Unified Representation for Mapping, Odometry, and Planning," *IEEE Transactions on Robotics*, pp. 1–17, 2023. [Online]. Available: <https://ieeexplore.ieee.org/document/10202666/>
- [8] C. L. Gentil, O.-L. Ouabi, L. Wu, C. Pradalier, and T. Vidal-Calleja, "Accurate Gaussian Process-based Distance Fields with applications to Echolocation and Mapping," Sep. 2023, arXiv:2302.13005 [cs] version: 2. [Online]. Available: <http://arxiv.org/abs/2302.13005>
- [9] B. Lee, C. Zhang, Z. Huang, and D. D. Lee, "Online continuous mapping using gaussian process implicit surfaces," in *2019 International Conference on Robotics and Automation (ICRA)*. IEEE, 2019.
- [10] U. Ali, L. Wu, A. Mueller, F. Sukkar, T. Kaupp, and T. Vidal-Calleja, "Interactive distance field mapping and planning to enable human-robot collaboration," *arXiv preprint arXiv:2403.09988*, 2024.
- [11] B. Lau, C. Sprunk, and W. Burgard, "Improved updating of euclidean distance maps and voronoi diagrams," in *2010 IEEE/RSJ International Conference on Intelligent Robots and Systems*. IEEE, 2010, pp. 281–286.
- [12] Y. Pan, Y. Kompis, L. Bartolomei, R. Mascaro, C. Stachniss, and M. Chli, "Voxfield: Non-Projective Signed Distance Fields for Online Planning and 3D Reconstruction," in *2022 IEEE/RSJ International Conference on Intelligent Robots and Systems (IROS)*. Kyoto, Japan: IEEE, Oct. 2022, pp. 5331–5338.
- [13] K. Museth, J. Lait, J. Johanson, J. Budsberg, R. Henderson, M. Alden, P. Cucka, D. Hill, and A. Pearce, "Openvdb: an open-source data structure and toolkit for high-resolution volumes," in *Acm siggraph 2013 courses*, 2013, pp. 1–1.
- [14] K. Museth, "Vdb: High-resolution sparse volumes with dynamic topology," *ACM transactions on graphics (TOG)*, vol. 32, no. 3, pp. 1–22, 2013.
- [15] K. Goel and W. Tabib, "Distance and collision probability estimation from gaussian surface models," *arXiv preprint arXiv:2402.00186*, 2024.
- [16] J. J. Park, P. Florence, J. Straub, R. Newcombe, and S. Lovegrove, "Deepsdf: Learning continuous signed distance functions for shape representation," in *Proceedings of the IEEE/CVF conference on computer vision and pattern recognition*, 2019, pp. 165–174.
- [17] A. Gropp, L. Yariv, N. Haim, M. Atzmon, and Y. Lipman, "Implicit geometric regularization for learning shapes," *arXiv preprint arXiv:2002.10099*, 2020.
- [18] M. Pantic, C. Cadena, R. Siegwart, and L. Ott, "Sampling-free obstacle gradients and reactive planning in neural radiance fields (nerf)," *arXiv preprint arXiv:2205.01389*, 2022.
- [19] J. Ortiz, A. Clegg, J. Dong, E. Sucar, D. Novotny, M. Zollhoefer, and M. Mukadam, "isdf: Real-time neural signed distance fields for robot perception," *arXiv preprint arXiv:2204.02296*, 2022.
- [20] J. Huang, S.-S. Huang, H. Song, and S.-M. Hu, "Di-fusion: Online implicit 3d reconstruction with deep priors," in *Proceedings of the IEEE/CVF Conference on Computer Vision and Pattern Recognition*, 2021, pp. 8932–8941.
- [21] V. Vasilopoulos, S. Garg, J. Huh, B. Lee, and V. Isler, "Hio-sdf: Hierarchical incremental online signed distance fields," *arXiv preprint arXiv:2310.09463*, 2023.
- [22] C. E. Rasmussen and C. K. Williams, *Gaussian Processes for Machine Learning*. Cambridge, Mass.: MIT Press, 2006.
- [23] W. E. Lorensen and H. E. Cline, "Marching cubes: A high resolution 3d surface construction algorithm," in *Proceedings of the 14th Annual Conference on Computer Graphics and Interactive Techniques*, ser. SIGGRAPH '87. Association for Computing Machinery, 1987.
- [24] B. Curless and M. Levoy, "A volumetric method for building complex models from range images," in *Proceedings of the 23rd Annual Conference on Computer Graphics and Interactive Techniques*, ser. SIGGRAPH '96. Association for Computing Machinery, 1996, p. 303–312.
- [25] M. Ramezani, Y. Wang, M. Camurri, D. Wisth, M. Mattamala, and M. Fallon, "The newer college dataset: Handheld lidar, inertial and vision with ground truth," in *2020 IEEE/RSJ International Conference on Intelligent Robots and Systems (IROS)*, 2020, pp. 4353–4360.



- [26] L. Mescheder, M. Oechsle, M. Niemeyer, S. Nowozin, and A. Geiger, "Occupancy networks: Learning 3d reconstruction in function space," in *Proceedings of the IEEE/CVF conference on computer vision and pattern recognition*, 2019, pp. 4460–4470.